Active extensile stress promotes 3D director orientations and flows

Mehrana R. Nejad[1] and Julia M. Yeomans[1]

[1] *The Rudolf Peierls Centre for Theoretical Physics, Department of Physics, University of Oxford, Parks Road, Oxford OX1 3PU, UK*

We use numerical simulations and linear stability analysis to study an active nematic layer where the director is allowed to point out of the plane. Our results highlight the difference between extensile and contractile systems. Contractile stress suppresses the flows perpendicular to the layer and favours in-plane orientations of the director. By contrast extensile stress promotes instabilities that can turn the director out of the plane, leaving behind a population of distinct in-plane regions that continually elongate and divide. Our results suggest a mechanism for the initial stages of layer formation in living systems, and explain the propensity of dislocation lines in three-dimensional active nematics to be of twist-type in extensile, or wedge-type in contractile, materials.

Living systems continuously receive energy from external sources and dissipate this energy by exerting forces on their surroundings and performing work [1]. Being out of equilibrium, these systems have a great potential to exhibit novel behaviors that cannot be captured by conventional equilibrium statistical mechanics [2]. Examples include coherent animal flocks [3], non-trivial rheological properties of active suspensions such as zero viscous resistance to shear flow [4], and cell crawling and division [5, 6]. The hydrodynamics of active particles, such as bacteria, cells and microtubules driven by kinesin motors lies in the low Reynolds number regime and they can be modeled as force dipoles with nematic symmetry. The direction of the force dipoles can be inwards along the dipolar axis (contractile systems) or outwards (extensile systems). Both extensile and contractile systems are found in nature: actomyosin suspensions are contractile, microtubule-kinesin motor suspensions and bacteria are extensile, while confluent cell layers can be either [7, 8].

Active stresses destabilise the nematic phase resulting in a state of chaotic flows, with prominent vorticity and fluid jets, known as active turbulence [9–16]. In two dimensions active turbulence is characterized by the continuous creation and annihilation of +1/2 and -1/2 topological defect pairs in the nematic director field [17–19]. The +1/2 defects have polar symmetry and hence are self-propelled. Recently, three-dimensional active suspensions have also attracted a considerable amount of interest. In contrast to 2D, 3D active flows are governed by the creation and annihilation of disclination lines and loops [20–22].

There is significant understanding of completely 2D or 3D active materials. However many biological systems evolve from 2D to 3D structures during their life cycle. The growth of a 2D layer into the third dimension leads to the formation of biofilms [23, 24], where the transition is often initiated by the formation of a vertically aligned core of bacteria [25, 26]. Gastrulation is a vital step in the early development of most animals when a single layer epithelium is reorganised into a multilayer structure of differentiated cells that will form specific tissues and organs [27].

To understand these processes further, in this paper we study the transition from 2D to 3D in active nematics showing that extensile and contractile materials demonstrate remarkably different behaviours. Extensile systems promote flows perpendicular to the layer and develop out-of-plane director orientations, but these coexist with dynamic, elongated, regions where the director remains in-plane. By contrast, contractile stresses suppress flow perpendicular to the layer and the contractile systems develop the usual 2D active turbulence.

Equations of motion: To study the role of active stresses on the transition from 2D to 3D, we consider an active nematic layer in the x-y plane. Allowing the director and velocity fields to have components along x, y and z directions, we numerically solve the active nematohydrodynamic equations of motion [28]. The nematic order is defined by the 3D tensor $\boldsymbol{Q} = 3\mathcal{S}\left(\boldsymbol{nn} - \boldsymbol{I}/3\right)/2$, with director field $\boldsymbol{n}$ and scalar order parameter $\mathcal{S}$, and evolves according to $D_t\boldsymbol{Q} - \boldsymbol{S} = \boldsymbol{H}/\gamma$ [29]. The nematic tensor relaxes towards equilibrium at a rate determined by the rotational viscosity γ and D_t and $\boldsymbol{S}$ describe the material derivative and co-rotational advection due to gradients of the velocity field [28].

The nematic equilibrium follows from the molecular field $\boldsymbol{H}$, which is a functional derivative of the free energy. The free energy density includes a Landau-de Gennes term $\mathcal{F}_{\text{bulk}} = \frac{A}{2}\boldsymbol{Q}^2 + \frac{B}{3}\boldsymbol{Q}^3 + \frac{C}{4}\boldsymbol{Q}^4$ where we choose the prefactors so that the equilibrium is in the nematic phase. We also include a distortion energy density that penalizes deformations in the orientation field, choosing the one-constant elastic approximation $\mathcal{F}_{\text{el}} = \frac{K}{2}\left(\boldsymbol{\nabla Q}\right)^2$.

The velocity field $\boldsymbol{u}$ obeys the incompressible Navier-Stokes equation $D_t\boldsymbol{u} = \boldsymbol{\nabla}\cdot\boldsymbol{\Pi}/\rho$, where ρ

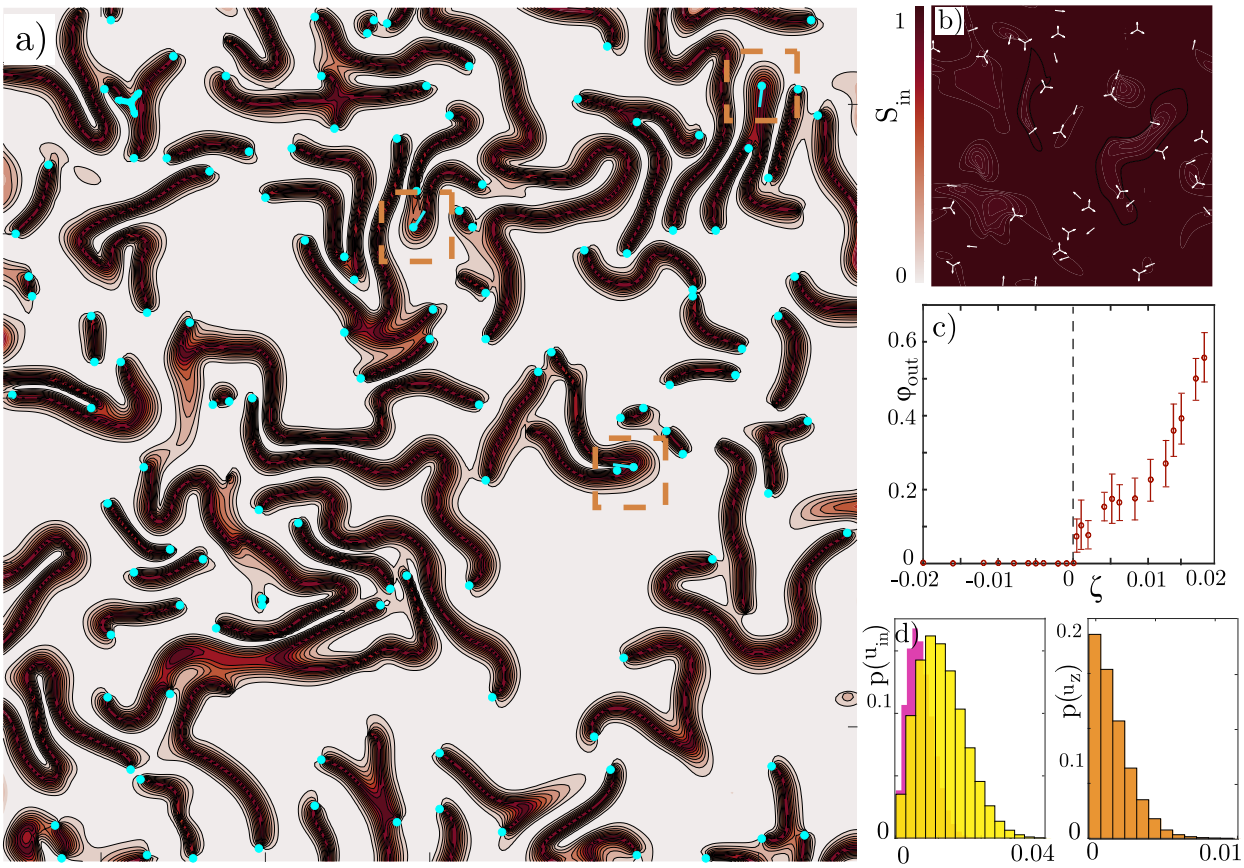

FIG. 1: Snapshots from simulations of 2D active nematics layers. Color denotes the magnitude of the in-plane order from in-plane (black) to out-of-plane (white): (a) extensile stress, 3D twist type and 2D wedge type defects are represented in cyan. (b) contractile stress, two-dimensional $\pm 1/2$ topological defects are shown in white. (c) Area fraction of regions with out of plane director as a function of activity. d) Histogram showing distribution of in-plane $u_{\rm in}$ and out-of-plane $u_{\rm z}$ velocities for contractile (yellow, $u_{\rm z} = 0$) and extensile (pink, orange) driving.

is the density and the generalized stress $\mathbf{\Pi}$ has viscous, elastic, and active components [30]. The active stress is described by $-\zeta \boldsymbol{Q}$ [31] where the divergence of $\boldsymbol{Q}$ drives active forcing which destabilises the nematic ordering. The equations of motion are solved using a hybrid lattice Boltzmann method [28]. Details of the values of the parameters and the full form of nematohydrodynamic equations can be found in the Supplemental Material (SM).

Results: In Fig. 1 we compare the behaviour of an extensile system with activity $\zeta = 0.008$ with that of a contractile system with $\zeta = -0.008$. The figure shows that contractile stresses suppress perturbations of the director field in the direction perpendicular to the layer, leading to the usual 2D active dynamics (Fig. 1(b)). In extensile systems, however, the director has non-zero out-of-plane components except within dynamic, elongated domains (Fig. 1(a) and Movie 1). This behaviour is quantified in Fig. 1(c) where we plot the area fraction of the out-of-plane regions as a function of activity, showing that this quantity remains zero for the contractile case, but increases with activity in extensile systems. Histograms of the corresponding in-plane and out-of-plane flow fields are shown in Fig. 1(d). In contractile systems flows remain in the x-y plane whereas in the extensile case the flow develops substantial components along z which act to drive the director into the third dimension.

We will discuss the dynamics of the in-plane domains in the extensile case below, but first we perform a linear stability analysis of the nematohydrodynamic equations around the fully-aligned in-plane nematic phase to further understand the different behaviour of extensile and contractile systems. Representing the Fourier transform of any fluctuating

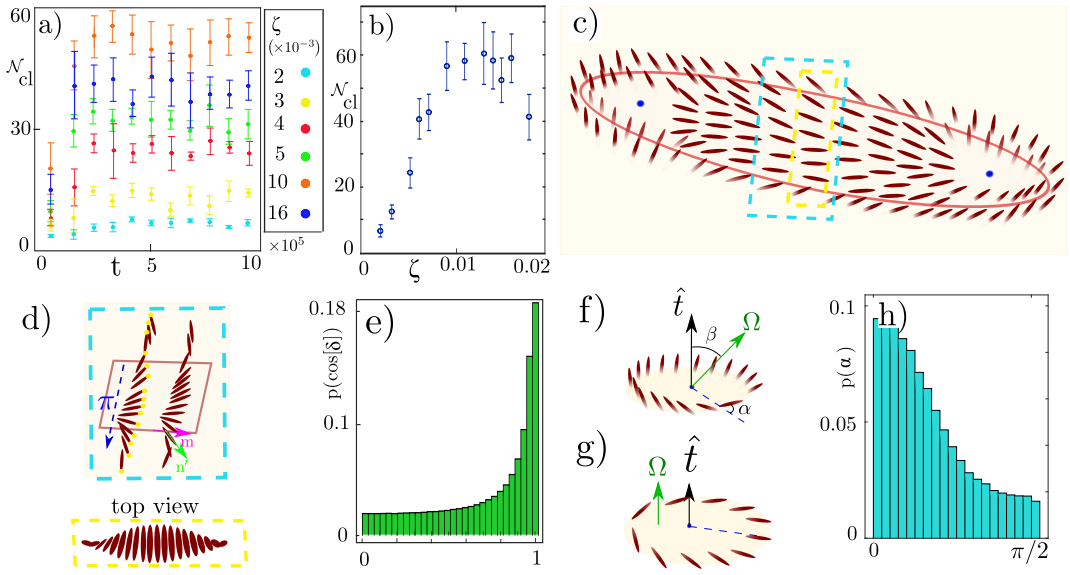

FIG. 2: a) The number of snakes reaches a steady state after a while. b) Represents the number of snakes as a function of activity at steady state. c) Represents the director in a snake. d) In going from out-of-plane to in-plane to out-of-plane domains, crossing the width of a snake, the director twists by π. e) Represents the distribution of the angle between the director and the tangent to the boundary of snakes. The histogram peaks at $\cos(\delta) = 1$, suggesting parallel alignment of the director with the boundary. f) and g) show 3D twist type and 2D wedge-type defects observed in extensile and contractile systems, respectively. The blue circles show the center of defects, $\hat{t}$ represents the normal to the layer, and the blue dashed line connects the center of the twist type defect to the region with in-plane director. The director around the rotation vector Ω. g) Represents the distribution of angle α in extensile systems.

field δf as $\delta f(\mathbf{r},t) = \int d\mathbf{q}\ \tilde{f}(\mathbf{q},\omega)\ e^{i\mathbf{q}\cdot\mathbf{r}+\omega t}$, in the long-wave-length and zero Reynolds number limit the growth rate of a perturbation reads:

$$\omega_{out} = \frac{3\zeta}{4\eta}\cos^2\theta,\ \ \omega_{in} = \frac{3\zeta}{4\eta}\cos 2\theta, \qquad (1)$$

where ω_{out} and ω_{in} are the growth rates of the out-of-plane and in-plane components of the director, θ is the angle between the wavevector of the perturbation and the direction of the order and η is the viscosity. Details of the calculations and the full form of the growth rates (including the flow-aligning dependence) can be found in the SM.

The onset of instability is given by the condition $\omega_{in/out} > 0$. The in-plane component shows the well-known instability of 2D active nematics to bend (splay) perturbations in extensile (contractile) systems [31]. By contrast the growth rate of the out-of-plane component does not change sign for different values of θ and is positive (negative) for extensile (contractile) systems. Thus the out-of-plane component only grows in extensile systems. Eq. (1) also shows that the growth rate of the out-of-plane component is maximum in places with in-plane bend perturbations ($\theta = 0, \pi$) and that it is zero in places with in-plane splay fluctuations ($\theta = \pi/2$).

In-plane domains in extensile active nematics: We now return to consider the elongated domains where the director field remains in the x-y plane. These initially form in regions of splay distortion where the flow fields along the z-axis are insufficiently strong to push the director field out of the plane. For convenience we will refer to the in-plane domains as *snakes*.

After a transient phase the average number of snakes fluctuates around a constant value (Fig. 2(a)) which first increases and then decreases with increasing activity (Fig. 2(b)). This reflects a balance between snakes elongating and then breaking up, and the possibility that local flows will be sufficiently strong to destroy a snake by pushing the director out of the x-y plane.

To understand how the snakes lengthen and divide we study their director and flow fields. We first measure $\cos\delta$, the angle between the orientation of the director at the boundary of a cluster and the local tangent to the boundary. The histogram of $\cos\delta$, shown in Fig. 1(e) peaks at $\cos\delta = 1$, showing that the director inside a snake tends to align parallel to

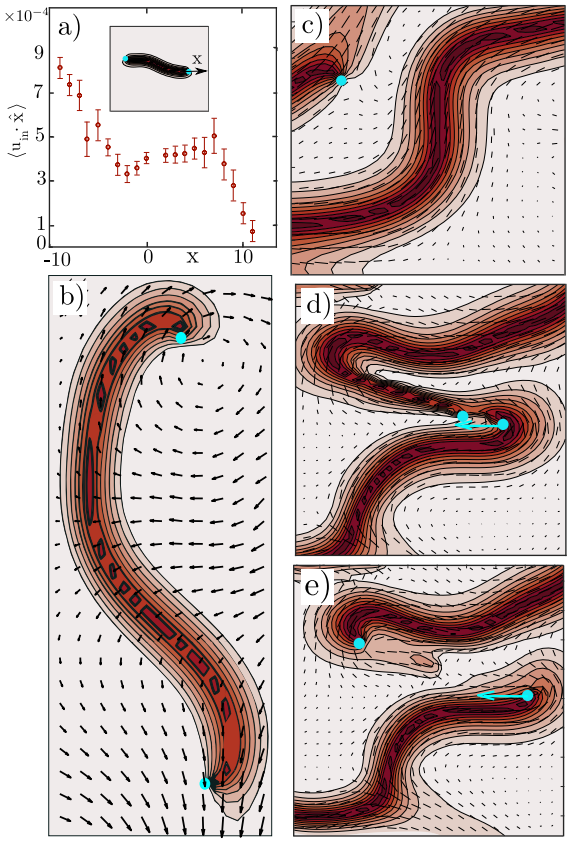

FIG. 3: a) Average flow along the direction of the elongation of snakes (measured at the edge). The flow is on average towards the end of the snakes ($\langle \mathbf{u}_{in} \cdot \hat{x} \rangle > 0$), indicating that active flows elongate the clusters. b) Flows around a snake. c)-e) Evolution of a snake. Elongated snakes undergo a bend instability and form defects. The snake then go to the third direction and divides to two snake with twist-type defects at their edge.

its long edges.

Therefore, along the boundaries of a snake the director rotates through $\pi/2$ to match the surrounding vertical director configuration (Fig. 2(d)) and as a result, looking at a cross-section of a snake, the director twists by π (Fig. 2(d)). At the ends of the snake this results in twist defects with the director configuration shown in Fig. 2(f). An angle which characterises twist defects is α (introduced in Fig. 2(f)). α shows the angle between the in-plane director around a defect and the line which connects the center of the defect to the position of the in-plane director. Fig. 2(h) shows that α has a peak at $\alpha = 0$, showing that the twist-type defects which form are predominantly radial. This agrees with the results from the linear stability analysis that defect heads (tails) where the bend (splay) deformation is large the director develops a component along z (stays in the x-y plane).

We are now in a position to understand the dynamics of a snake. The stresses which results from the twist defects set up flows which act to elongate the snakes and to align the director field inside them (Fig. 3(a),(b)). The ensuing evolution is illustrated in Figs. 3(c)-(e). Since the system is extensile and the director is parallel to their length, the elongated snakes undergo a bend instability (see Movie 1). The growth of a bend deformation is equivalent to the formation of a pair of two-dimensional, $\pm 1/2$ defects (orange outlines in Fig. 1(a) and Fig. 3(c)-(e)). We have seen that bend deformations are unstable to director perturbations perpendicular to the layer and, due to the large bend deformations at the position of the defects, the director rotates out of the plane and the snake splits into two smaller snakes terminated by twist director configurations.

Relation to 3D active turbulence: The behavior that we have identified in two dimensions persists into three dimensions. Fully-developed 3D active turbulence is characterised by motile disclination lines that form closed loops that can appear, grow, shrink and disappear [20–22]. The director configuration on a plane locally perpendicular to a dislocation line can be characterised by the twist angles $\beta = \cos^{-1}(\hat{t} \cdot \hat{\Omega})$ [22] where $\hat{t}$ is the unit tangent to the disclination line and $\hat{\Omega}$ shows the direction around which the director rotates. $\beta = 0, \pi$ (or equivalently $\hat{\Omega} = \hat{t}$) correspond to cross sections of the dislocation line with the configurations of $-1/2$ and $+1/2$ defects respectively, and other values indicate degrees of twist where the director rotates out of the plane (see Fig. 2(e)). Fig. 4(a)-(b) compares the distribution of β for the single layer considered here to simulations of full 3D active turbulence keeping the activity the same, and considering both extensile and contractile systems. The figure shows that similar behaviour is observed in both cases: in contractile systems defects are predominantly two dimensional, whereas in the extensile system there is a clear preference for introducing twist type defects.

The transition from 2D to 3D is a vital step in many biological processes. Biofilm formation can be initiated by cells turning to point at right angles to the substrate [23–26]. This has been described in terms of mechanical instabilities due to in-plane compression resulting from cell divisions or effective interactions between bacteria. However, noting that bacterial division is a source of extensile stress, the mechanism we introduce here provides another pos-

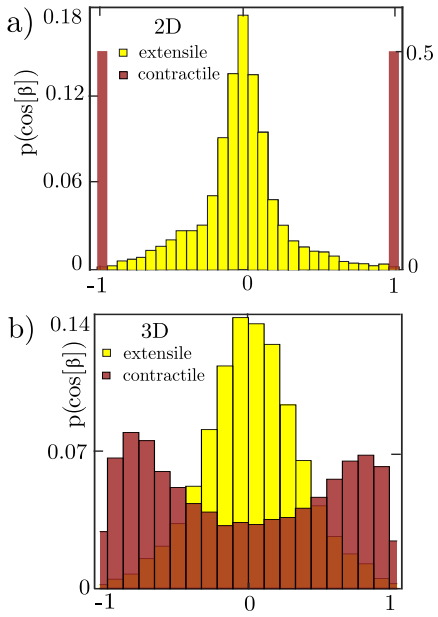

FIG. 4: Twist angle β in (a) 2D, (b) 3D. In extensile system most defects are twist-type ($\beta = \pi/2$) while in contractile systems most defects are wedge-type ($\beta = 0, \pi$).

sible route to cell verticalization.

Epithelial layers evolve into 3D configurations during embryogenesis; examples are the ingression of cells at the primitive streak in the chick embryo [32] and the inward folding of an epithelial sheet in the fruit fly embryo [33]. Our work suggests that localised activity and cell divisions might play a role in the formation of these structures.

ACKNOWLEDGEMENTS

M.R.N. acknowledges the support of the Clarendon Fund Scholarships.

[1] S. Ramaswamy, Journal of Statistical Mechanics: Theory and Experiment **2017**, 054002 (2017).
[2] M. C. Marchetti, J. F. Joanny, S. Ramaswamy, T. B. Liverpool, J. Prost, M. Rao, and R. A. Simha, Rev. Mod. Phys. **85**, 1143 (2013).
[3] A. Cavagna and I. Giardina, Annual Review of Condensed Matter Physics **5**, 183 (2014).
[4] H. M. López, J. Gachelin, C. Douarche, H. Auradou, and E. Clément, Phys. Rev. Lett. **115**, 028301 (2015).
[5] A. Farutin, J. Étienne, C. Misbah, and P. Recho, Phys. Rev. Lett. **123**, 118101 (2019).
[6] S. M. Rafelski and J. A. Theriot, Annual Review of Biochemistry **73**, 209 (2004).
[7] L. Balasubramaniam, A. Doostmohammadi, T. B. Saw, G. H. N. S. Narayana, R. Mueller, T. Dang, M. Thomas, S. Gupta, S. Sonam, A. S. Yap, *et al.*, Nature Materials , 1 (2021).
[8] G. Duclos, C. Blanch-Mercader, V. Yashunsky, G. Salbreux, J.-F. Joanny, J. Prost, and P. Silberzan, Nature Physics **14**, 728 (2018).
[9] S. Fraden, Nat. Phys. **15**, 311 (2019).
[10] J. Dunkel, S. Heidenreich, K. Drescher, H. H. Wensink, M. Bär, and R. E. Goldstein, Phys. Rev. Lett. **110**, 228102 (2013).
[11] H. H. Wensink, J. Dunkel, S. Heidenreich, K. Drescher, R. E. Goldstein, H. Löwen, and J. M. Yeomans, Proceedings of the National Academy of Sciences **109**, 14308 (2012).
[12] J. Słomka and J. Dunkel, Proceedings of the National Academy of Sciences **114**, 2119 (2017).
[13] B. Martínez-Prat, J. Ignés-Mullol, J. Casademunt, and F. Sagués, Nature Physics **15**, 362 (2019).
[14] C. Blanch-Mercader, V. Yashunsky, S. Garcia, G. Duclos, L. Giomi, and P. Silberzan, Phys. Rev. Lett. **120**, 208101 (2018).
[15] L. M. Lemma, S. J. DeCamp, Z. You, L. Giomi, and Z. Dogic, Soft Matter **15**, 3264 (2019).
[16] S. P. Thampi, A. Doostmohammadi, T. N. Shendruk, R. Golestanian, and J. M. Yeomans, Science Advances **2** (2016).
[17] D. Cortese, J. Eggers, and T. B. Liverpool, Phys. Rev. E **97**, 022704 (2018).
[18] V. Schaller and A. R. Bausch, Proc. Natl. Acad. Sci. U.S.A **110**, 4488 (2013).
[19] K. Thijssen, M. R. Nejad, and J. M. Yeomans, Phys. Rev. Lett. **125**, 218004 (2020).
[20] G. Duclos, R. Adkins, D. Banerjee, M. S. Peterson, M. Varghese, I. Kolvin, A. Baskaran, R. A. Pelcovits, T. R. Powers, A. Baskaran, *et al.*, Science **367**, 1120 (2020).
[21] J. Binysh, J. Pollard, and G. P. Alexander, Phys. Rev. Lett. **125**, 047801 (2020).
[22] J. Binysh, i. c. v. Kos, S. Čopar, M. Ravnik, and G. P. Alexander, Phys. Rev. Lett. **124**, 088001 (2020).
[23] R. Hartmann, P. K. Singh, P. Pearce, R. Mok, B. Song, F. Díaz-Pascual, J. Dunkel, and K. Drescher, Nature Physics **15**, 251 (2019).
[24] Z. You, D. J. Pearce, A. Sengupta, and L. Giomi, Physical Review Letters **123**, 178001 (2019).
[25] M. R. Warren, H. Sun, Y. Yan, J. Cremer, B. Li, and T. Hwa, ELife **8**, 41093 (2019).
[26] F. Beroz, J. Yan, Y. Meir, B. Sabass, H. A. Stone, B. L. Bassler, and N. S. Wingreen, Nature Physics **14**, 954 (2018).
[27] L. Solnica-Krezel, *Gastrulation: From embryonic pattern to form*, Vol. 136 (Academic Press, 2020).
[28] D. Marenduzzo, E. Orlandini, M. Cates, and J. M. Yeomans, Physical Review E **76**, 031921 (2007).
[29] A. N. Beris and B. J. Edwards, *Thermodynamics of flowing systems: with internal microstructure*, 36 (Oxford University Press, 1994).

[30] D. Marenduzzo, E. Orlandini, and J. M. Yeomans, Phys. Rev. Lett. **98**, 118102 (2007).
[31] R. A. Simha and S. Ramaswamy, Phys. Rev. Lett. **89**, 058101 (2002).
[32] G. S. Nájera and C. J. Weijer, Mechanisms of Development **163**, 103624 (2020).
[33] A. C. Martin, Genetics **214**, 543 (2020).